Three coupled oscillators as a universal probe of synchronization stability in coupled oscillator arrays

Kenneth S. Fink

Columbia University, New York, New York 10027

Gregg Johnson, Tom Carroll, Doug Mar, and Lou Pecora

Code 6340, Naval Research Laboratory, Washington, D.C. 20375

(Received 4 May 1999)

We show that the stability surface that governs the synchronization of a large class of arrays of identical oscillators can be probed with a simple array of just three identical oscillators. Experimentally this implies that it may be possible to probe the synchronization conditions of many arrays all at the same time. In the process of developing a theory of the three-oscillator probe, we also show that several regimes of asymptotic coupling can be derived for the array classes, including the case of large imaginary coupling, which apparently has not been explored.

PACS number(s): 05.45.−a

I. INTRODUCTION

In this paper we show a special form of coupling between three identical oscillators which allows us to probe a general stability function that determines the stability of the synchronous state of a very large class of arrays of identical oscillators. The three-coupled system is, in that sense, a universal probe of the stability of synchronization in practically any array of similar oscillators connected by a wide range of couplings. We show the development of this three-oscillator system by first reviewing the derivation of the master stability function for general arrays of identical oscillators.

The increasing interest in synchronization in dynamical systems, whether chaotic or periodic, has led many people to consider the phenomenon of synchronization in large arrays or networks of coupled oscillators [1–16]. A central dynamical question is, when is such synchronous behavior stable, especially in regard to coupling strengths and connectivity in the network?

Many approaches have been tried in solving the synchronization problem, often with emphasis on a particular coupling scheme, but ocassionally with a view to understanding general patterns of synchronization criteria that could be applied to whole classes of oscillator networks (see, for example, Refs. [1], [5], [17–25]). Most of the networks can be classified as a collection of identical nodes (oscillators) in which the same component is taken from each node and applied to other nodes in the network with various weights which depend on the node pairs that are coupled. The use of node components can be relaxed, more generally, using a function of the node dynamical variables as the output of each node to be fed to the other nodes. The weights are applied to each output as a whole and are often kept constant for simplicity.

We have shown that we can solve a very general form of the problem of the stability of the synchronized state in oscillators coupled as described above [26]. We have solved this problem once and for all for any set of coupling weights and connections and any number of coupled oscillators, given the particular oscillator type at each node and the func-

tional form through which the nodes are coupled. Note: we assume nothing about the motion off the synchronization manifold, since that will not affect the linear stability analysis. Although the above description of the system is rather wordy, the equations of motion and, most importantly, the variational equations used in the stability analysis, have a compact form that leads quickly to a general solution of the stability problem. We call the general solution the *master stability function* [26]. It is this master stability function that our three-oscillator system will probe.

We note that several other works by Hu, Yang, and Liu [25] and Gade and co-workers [23,24] used some of the techniques we present here, especially in the application of eigenvalues of the connectivity matrix to random and star coupling configuration. Our work independently developed the master stability function for the general case, and herein shows how it can be used to predict many of the phenomena and characteristics of dynamics near the synchronous state.

In the following sections we derive the variational problem leading to the master stability function (MSF). We also show how the asymptotic (large real and imaginary coupling) form of the MSF can be derived. Then we show that a properly constructed three-oscillator system can probe the MSF by a simple variation of the couplings. This allows the MSF to be explored experimentally as well as numerically. We go on to show an experimental investigation of the MSF for Rössler-like circuits, which discloses the stable regions of the MSF and brings into question the appropriate stability criterion to use in real systems. We show that many other synchronization stability criteria have an associated MSF. Finally, in the Appendix, we show that there is also a MSF for coupled map lattices.

II. STABILITY ANALYSIS

We assume the following: (1) The coupled oscillators (nodes) are all identical. (2) The same function of the components from each oscillator is used as an output to couple to other oscillators. (3) The synchronization manifold is an invariant manifold. (4) The nodes are coupled in an arbitrary

fashion which is well approximated near the synchronous state by a linear operator. Assumptions (1) and (3) guarantee the existence of a synchronization hyperplane in phase space, and assumption (2) makes the stability function (MSF) specific to our choice of oscillators and the output function. Assumption (4) is the choice of many studies of coupled systems, but note that the linear coupling form is necessary only near the synchronization manifold. It can be arbitrary elsewhere.

In determining the stability of the synchronous state, various criteria are possible. The weakest is that the maximum Lyapunov exponent or Floquet exponent be negative. This is a universal stability standard, but it does not guarantee that there are not unstable invariant sets in the synchronous state [7] or areas on the attractor that are locally unstable [10,27,28], both of which can cause attractor bubbling and bursting of the system away from synchronization when there is noise or parameter mismatch. The theory we develop below will apply to almost any criterion that depends on the variational equation of the system. Each stability criterion will lead to its own master stability function. For that reason we develop the theory in the context of Lyapunov exponents as a stability criterion and show in the conclusions how the other criteria can be used.

Let there be N nodes (oscillators). Let $\mathbf{x}^i$ be the m-dimensional vector of dynamical variables of the ith node. Let the dynamics for each node be

$$\dot{\mathbf{x}}^i = F^i(\mathbf{x}^i, \mathbf{H}(\mathbf{x})). \tag{1}$$

$\mathbf{H}: R^m \rightarrow R^m$ is an arbitrary output function of each node's variables that is used in the coupling. We collect node dynamical variables in $\mathbf{x} = (\mathbf{x}^1, \mathbf{x}^2, \ldots, \mathbf{x}^N)$, and write $\mathbf{H}(\mathbf{x}) = (\mathbf{H}(\mathbf{x}^1), \mathbf{H}(\mathbf{x}^2), \ldots, \mathbf{H}(\mathbf{x}^N))$, i.e., $\mathbf{H}$ is the same for all nodes. For example, we may have ''y coupling'' of three-dimensional oscillator nodes by choosing $\mathbf{H}$ as a matrix such that $H_{22} = 1$ and all other $H_{ij} = 0$. In this way the y component for each node is fed into the vector field for the ith node. At this point the actual functional dependence of $\mathbf{F}$ on the components $(\mathbf{H}(\mathbf{x}))$ is left unspecified. It is this latter functional dependence that defines the connectivity and coupling strengths of the network.

The $N-1$ constraints $\mathbf{x}^1 = \mathbf{x}^2 = \cdots = \mathbf{x}^N$ define the *synchronization manifold*. To test the stability of the motion in the synchronous state, we must evaluate the Lyapunov exponents of directions transverse to the synchronization manifold. We want perturbations in the transverse directions to damp out (have negative Lyapunov exponents). This requires sorting out the transverse directions from the synchronization manifold directions in the variational equation. We show how this comes about naturally in our development of a master stability function.

The variational equations for the coupled system are

$$\dot{\xi}_i = \mathbf{J} \cdot \xi_i + \sum_{j=1}^{N} D_j \mathbf{F}^i \cdot D\mathbf{H} \xi_j, \tag{2}$$

where ξ_j are the (m-dimensional) perturbations of the jth node; $\mathbf{J}$ is the usual Jacobian of any node (the derivative with respect to the first argument of $\mathbf{F}^i$, which is the same for all nodes in the synchronous state); $D_j \mathbf{F}^i$ is the derivative (an

$m \times m$ matrix) with respect to the jth perturbation in the coupling term $\mathbf{H}(x)$ in $\mathbf{F}^i$; and $D\mathbf{H}$ is the Jacobian of the coupling function evaluated at each node (which is the same for all nodes in the synchronous state).

At this stage we constrain the dependence of $\mathbf{F}^i$ on $\mathbf{H}(\mathbf{x})$ to be as follows. Near the synchronization manifold we want this dependence to be dominated by linear terms; thus, near synchronization, each $D_j \mathbf{F}^i$ should approach the form $\Sigma_j \mathbf{G}_{ij} D\mathbf{H} \xi_j$, where $\mathbf{G}_{ij}$ is a constant $m \times m$ matrix. We also want the coupling to give equal weighting to all components of $D\mathbf{H}$, that is, $D\mathbf{H} \xi_j$ is added in Eq. (2) to the sum using a scalar weight. The latter constraint requires that $\mathbf{G}_{ij}$ be a multiple of the $m \times m$ unit matrix: $\mathbf{G}_{ij} = G_{ij} \mathbf{1}_m$. These constraints are quite general, and cover many of the coupling schemes found in the literature.

With the above constraints we can write Eq. (2) in a compact form using direct products of matrices,

$$\dot{\xi} = [\mathbf{1}_N \otimes \mathbf{J} + \mathbf{G} \otimes D\mathbf{H}] \xi, \tag{3}$$

where $\xi = (\xi_1, \xi_2, \ldots, \xi_N)$ is the collection of perturbations of all the coupled oscillators, $\mathbf{G}$ is the matrix of scalar weights, G_{ij}, and $\mathbf{1}_N$ is the $N \times N$ identity matrix. Recall that the direct product of two matrices $\mathbf{A}$ and $\mathbf{B}$ is given in block form by

$$\mathbf{A} \otimes \mathbf{B} = \begin{pmatrix} A_{11}\mathbf{B} & A_{12}\mathbf{B} & \cdots & A_{1N}\mathbf{B} \\ A_{21}\mathbf{B} & A_{22}\mathbf{B} & \cdots & A_{2N}\mathbf{B} \\ \vdots & \vdots & \vdots & \vdots \\ A_{N1}\mathbf{B} & A_{N2}\mathbf{B} & \cdots & A_{NN}\mathbf{B} \end{pmatrix}. \tag{4}$$

Note that manifold invariance [requirement (3) above] requires $\Sigma_j G_{ij} = 0$.

From the above assumptions the $\mathbf{G}$ matrix is constant on the synchronization manifold. This is true for any linear coupling scheme, and will be true for many other coupling schemes considered in the literature. This means the matrix $\mathbf{S}$ that diagonalizes $\mathbf{G}$ is a constant, and can be applied directly to the variational equation [Eq. (3)] at all points in the synchronization manifold. To apply $\mathbf{S}$ we recall the rules for block matrix manipulations using direct products [29]: (1) $\mathbf{A} \otimes \mathbf{B} \cdot \mathbf{C} \otimes \mathbf{D} = \mathbf{A} \cdot \mathbf{C} \otimes \mathbf{B} \cdot \mathbf{D}$ and (2) $(\mathbf{A} \otimes \mathbf{B})^{-1} = \mathbf{A}^{-1} \otimes \mathbf{B}^{-1}$. Thus the matrix $\mathbf{S} \otimes \mathbf{1}_m$ block diagonalizes the second term in Eq. (3), and leaves the first term untouched (it is already block diagonal with $\mathbf{J}$ in each $m \times m$ diagonal block). The block diagonalization uncouples the variational equations into blocks (analogous to a mode analysis) and we are left with variational equations

$$\dot{\xi}_k = [\mathbf{J} + \gamma_k D\mathbf{H}] \xi_k. \tag{5}$$

where γ_k is the eigenvalue of $\mathbf{G}$ for the kth block, and $k = 0, 1, 2, \ldots, N-1$. For $k=0$ we have the variational equation for the synchronization manifold ($\gamma_0 = 0$), which is required by synchronization manifold invariance ($\Sigma_j G_{ij} = 0$). All other k's correspond to transverse eigenvectors, so we have succeeded in separating the synchronization manifold from the other, transverse directions. We can think of these as transverse *modes*, and we will refer to them as such.
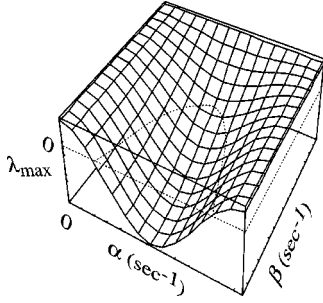
FIG. 1. Master stability function schematic. Here the stable region is the central valley, with the dotted lines separating the regions of stable and unstable synchronized behavior.

We now make an important observation: For each k the form of each block [Eq. (6)] is the same, with only the scalar multiplier γ_k differing for each. This leads us to the following formulation of the *master stability equation* and the associated *master stability function* (MSF): we calculate the maximum Floquet or Lyapunov exponent $\lambda_{\max}$ for the generic variational equation

$$\dot{\zeta} = [\mathbf{J} + (\alpha + i\beta)D\mathbf{H}]\zeta \qquad (6)$$

as a function of α and β (a point in the complex plane). This yields the master stability function $\lambda_{\max}$ as a surface over the complex plane (see Fig. 1 as an example). Complex numbers are used since $\mathbf{G}$ may have complex eigenvalues. Then, given a coupling or connection matrix $\mathbf{G}$, we locate the point γ_k in the complex plane. The sign of $\lambda_{\max}$ at that point will reveal the stability of that eigenmode—hence we have a MSF. If all the eigenmodes are stable, then the synchronous state is stable for that coupling scheme.

Interpretation of the complex coupling constant $(\alpha + i\beta)$ may seem difficult at first, but it is easy to associate a coupling scheme each with the real and imaginary part of the MSF coupling constant. If we have real coupling ($\beta = 0$ and $\alpha < 0$), the connection matrix $\mathbf{G}$ must be symmetric. For example, given two coupled oscillators

$$\frac{d\mathbf{x}^1}{dt} = \mathbf{F}(\mathbf{x}^1) + c(\mathbf{x}^2 - \mathbf{x}^1),$$

$$ \qquad (7)$$

$$\frac{d\mathbf{x}^2}{dt} = \mathbf{F}(\mathbf{x}^2) + c(\mathbf{x}^1 - \mathbf{x}^2),$$

where c is a scalar, we have $\mathbf{H} = \mathbf{1}_m$ and

$$\mathbf{G} = \begin{pmatrix} -c & c \\ c & -c \end{pmatrix}. \qquad (8)$$

The eigenvalues of $\mathbf{G}$ are 0 (on the synchronization manifold) and $-2c$. This is just what we get when we ''rotate'' by 45° to a new coordinate system ($\mathbf{x}_\parallel$ and $\mathbf{x}_\perp$) parallel and orthogonal to the synchronization manifold: $\mathbf{x}_\parallel = \mathbf{x}^1 + \mathbf{x}^2$ and $\mathbf{x}_\perp = \mathbf{x}^2 - \mathbf{x}^1$ [10,30]. Hence, symmetric coupling ($\mathbf{G}$) results in real eigenvalues, like $-2c$, which are interpreted as *damping*.

To understand the origin of imaginary eigenvalues, we first note we need three oscillators if there is an imaginary eigenvalue. This is because we still must have 0 as an eigenvalue and any complex eigenvalue must also have the complex conjugate present. Thus we should expect a diagonalized $\mathbf{G}$ matrix like

$$\mathbf{G}_{\text{diag}} = \begin{pmatrix} 0 & 0 & 0 \\ 0 & i & 0 \\ 0 & 0 & -i \end{pmatrix}. \qquad (9)$$

A simple similarity transformation on the 2×2 subblock in $\mathbf{G}_{\text{diag}}$ gives a matrix with real components:

$$\mathbf{G}'_{\text{diag}} = \begin{pmatrix} 0 & 0 & 0 \\ 0 & 0 & -1 \\ 0 & 1 & 0 \end{pmatrix}. \qquad (10)$$

Thus we see that imaginary coupling or imaginary eigenvalues of $\mathbf{G}$ come from antisymmetric connections, and the interpretation of such couplings is that they cause not a damping, but a *rotation* between two eigenmodes. The $\mathbf{G}$ matrix that associates with Eqs. (9) and (10) is

$$\mathbf{G} = \begin{pmatrix} 0 & -1/\sqrt{3} & 1/\sqrt{3} \\ 1/\sqrt{3} & 0 & -1/\sqrt{3} \\ -1/\sqrt{3} & 1/\sqrt{3} & 0 \end{pmatrix}. \qquad (11)$$

Note that this $\mathbf{G}$ is fully antisymmetric, and has zero row sums as required. We will return to these simple connection matrices later when we develop our three-oscillator universal probe.

III. ASYMPTOTIC COUPLING RESULTS

Obviously one way to determine the MSF $\lambda_{\max}(\alpha + i\beta)$ is to use traditional numerical techniques for finding Lyapunov exponents and apply them to the generic, master variational equation (6). This was done in Ref. [26], and will be done below for our special case, but here we introduce techniques that can lead to determination of the asymptotic form of $\lambda_{\max}$ for large (negative) real (α) and large imaginary (β) values.

Large and negative real coupling values in Eq. (6) can sometimes be treated as follows (we set $\beta = 0$ for now). Assume the case of a constant $D\mathbf{H}$ matrix. Then we can diagonalize $D\mathbf{H}$ everywhere on the synchronization manifold, and we end up with the variational equation,

$$\frac{d\boldsymbol{\psi}}{dt} = [\mathbf{K} + \alpha \, \text{diag}\{\eta_1, \ldots, \eta_m\}] \cdot \boldsymbol{\psi}, \qquad (12)$$

where $\mathbf{K}$ is the original Jacobian $\mathbf{J}$ after the similarity transformation that diagonalized $D\mathbf{H}$ and $\boldsymbol{\psi}$ is the transformed perturbation vector ζ. The matrix $\text{diag}\{\eta_1,...,\eta_m\}$ is the diagonal form of $D\mathbf{H}$, and we assume the eigenvalues η_i of $D\mathbf{H}$ are arranged in descending order ($\eta_1 > \eta_2 > \cdots$). Obviously we demand that since we are considering large, negative α

we must have all $\eta_i \geq 0$. If all η_i are strictly greater than zero, then we automatically have the results, that for large negative α, the variational rate must decrease linearly in α as $\alpha \eta_m$. Hence, for large real coupling there would always be stable behavior.

The case when $\eta_j = \eta_{j+1} = \eta_{j+2} = \ldots = \eta_m = 0$ for some value of j is more interesting. Then we have the situation that the first $j-1$ perturbation components $(\psi_1, \psi_2, \ldots, \psi_{j-1})$ damp out quickly to zero values, but the stability of the last $m-j+1$ components is determined by a subblock of the transformed Jacobian **K**. That subblock is given by the matrix,

$$\begin{pmatrix} K_{jj} & \cdots & K_{jm} \\ \vdots & \vdots & \vdots \\ K_{mj} & \cdots & K_{mm} \end{pmatrix}. \qquad (13)$$

This form of the stability equation obtains because the zero values of $(\psi_1, \psi_2, \ldots, \psi_{j-1})$ mean the components of **K** with either index less than j will not contribute to the vector field of the remaining $(\psi_j, \psi_{j+1}, \ldots, \psi_m)$ components, and the zeros of the eigenvalues will eliminate the coupling terms. Now the question of the asymptotic form of the MSF along the real axis is answered. It is a constant for small to moderate β values and its value is the largest ''Lyapunov exponent'' of the subblock of **K** [Eq. (13)].

We often refer to the subblock Lyapunov exponents as *conditional Lyapunov exponents* following our original work [31–33]. A simple example shows how this works. Assume we want to calculate the MSF for arrays of coupled Rössler systems. The equations of motion for the Rössler system are

$$\frac{dx}{dt} = -(y+z),$$

$$\frac{dy}{dt} = x + ay, \qquad (14)$$

$$\frac{dz}{dt} = b + z(x-c),$$

where we choose $a = b = 0.2$ and $c = 7.0$, a chaotic regime of behavior. Suppose we choose to couple our nodes using the x component. Then

$$\mathbf{H} = D\mathbf{H} = \begin{pmatrix} 1 & 0 & 0 \\ 0 & 0 & 0 \\ 0 & 0 & 0 \end{pmatrix} \qquad (15)$$

and we immediately see that the ''x component'' of the perturbation ζ will damp to zero for large, negative α, and we will be left with the yz subblock of the Jacobian of Eq. (15):

$$\begin{pmatrix} a & 0 \\ 0 & x-c \end{pmatrix}. \qquad (16)$$

It is easy to show that the value of x is usually less than c and

therefore the maximum conditional exponent is a which is positive. Thus the MSF for the Rössler must asymptote to an unstable level equal to a, as we also showed in previous work on diffusively coupled systems [5,34].

The case of large imaginary coupling is apparently a topic that has not been touched in the literature. We show how this regime can be approached for the MSF. First note that we simply want β large in either a positive or negative sense, since the MSF must be symmetric about the real axis. For now set $\alpha = 0$. As we noted above, imaginary coupling amounts to a rotation. Then large β can be associated with rapid oscillations. This association will allow us to obtain a general asymptotic result.

As for the large real coupling, we assume $D\mathbf{H}$ is a constant matrix with the same eigenvalue-eigenvector notation as above. We again diagonalize the Jacobian **J**, and obtain a variational equation:

$$\frac{d\boldsymbol{\psi}}{dt} = [\mathbf{K} + i\beta \, \text{diag}\{\eta_1, \ldots, \eta_m\}] \cdot \boldsymbol{\psi}. \qquad (17)$$

We assume that for some j $\eta_j = \eta_{j+1} = \eta_{j+2} = \cdots = \eta_m = 0$, whereas $\eta_i \neq 0$ for $i < j$. This condition on the η_j's simply means the last $m-j+1$ modes of each oscillator are not coupled to any other oscillator; only the first modes are physically coupled in the array. Since we can interpret $i\beta$ as causing rapid oscillation, we assume a solution in the following forms:

$$\psi_i = \phi_i e^{i\beta\eta_i t} \quad \text{when} \quad i < j,$$

$$\qquad (18)$$

$$\psi_i = \phi_i \quad \text{when} \quad i \geq j.$$

Substitution into Eq. (17) gives the following two forms of the variational equations:

$$\dot{\phi}_i = \sum_{l=1}^{m} K_{il} \phi_l e^{i\beta(\eta_l - \eta_i)t} \quad \text{when} \quad i < j, \qquad (19)$$

$$\dot{\phi}_i = \sum_{l=1}^{m} K_{il} \phi_l e^{i\beta\eta_l t} \quad \text{when} \quad i \geq j. \qquad (20)$$

Recall that β is arbitrarily large. This means the exponential terms involving β and nonzero eigenvalue combinations will oscillate arbitrarily fast on the time scale of the variational system. We invoke the technique of the method of averaging for differential equations [35], in which we can ''average'' in time over rapidly oscillating terms. In this case since the oscillations are so rapid the other factors are practically constant during any averaging time window, and the averaging will cause any terms with nonzero exponentials to vanish. For Equation (19) this means the only terms to survive in the sums are those for which $i = l$ (we are assuming no degeneracy of eigenvalues for now). For Eq. (20) this means only terms for which $l \geq j$ survive since, for those, by assumption, $\eta_l = 0$. If we now allow α to be nonzero, but not large we are left with the asymptotic block form for the variational equations:

$$\dot{\boldsymbol{\phi}}=\begin{pmatrix} K_{11}+\alpha & 0 & \cdots & 0 & \\ 0 & K_{22}+\alpha & \cdots & 0 & 0 \\ \vdots & \vdots & \vdots & \vdots & \\ 0 & 0 & \cdots & K_{j-1j-1}+\alpha & \\ & & & & K_{jj} & \cdots & K_{jm} \\ & & 0 & & \vdots & \vdots & \vdots \\ & & & & K_{mj} & \cdots & K_{mm} \end{pmatrix}\boldsymbol{\phi}, \qquad (21)$$

where $\boldsymbol{\phi}=(\phi_1,\phi_2,\ldots,\phi_m)$. The upper-left block is diagonal so the exponents of that block are associated with $j-1$ one-dimensional variational equations. Those exponents depend on α (which is negative). The lower-right block is the same as for the large real coupling case above. In fact, as $\alpha\to-\infty$, Eq. (21) approaches the same form as for the real case above, since the exponents associated with the upper-left block will all become large and negative and only the conditional exponents of the lower-right block will matter. Thus the imaginary asymptotic case transforms smoothly into the real asymptotic case.

As an example of large imaginary coupling, we again use the Rössler system with a, b, and c as above as our node system, but this time we couple through the y components:

$$\mathbf{H}=\begin{pmatrix} 0 & 0 & 0 \\ 0 & 1 & 0 \\ 0 & 0 & 0 \end{pmatrix}\cdot\mathbf{x}^j \Rightarrow D\mathbf{H}=\begin{pmatrix} 0 & 0 & 0 \\ 0 & 1 & 0 \\ 0 & 0 & 0 \end{pmatrix}, \qquad (22)$$

which gives the block formulation for large imaginary coupling,

$$\dot{\boldsymbol{\zeta}}=\begin{pmatrix} 0 & 0 & 1 \\ 0 & a+\alpha & 0 \\ z & 0 & x-c \end{pmatrix}\boldsymbol{\zeta}, \qquad (23)$$

where the y component is the diagonal block and the conditional block is the xz subsystem. If λ_{xz} is the maximum Lyapunov exponent of the xz subsystem then the asymptotic MSF is given as

$$\lambda_{\max}=\max\{a+\alpha,\lambda_{xz}\}. \qquad (24)$$

The conditional value of λ_{xz} is -0.022. Thus the MSF must look like Fig. 2. It starts out positive at $\alpha=0$ with a value of 0.2, then decreases linearly with α until it comes to the λ_{xz} value and levels out. Because we have chosen the maximum Lyapunov exponent, we are actually viewing a cross section of two Lyapunov exponent surfaces over the complex plane, one associated with the y diagonal and one associated with the xz subsystem. In general, the entire complex plane is covered by three surfaces, since the Lyapunov exponent spectrum has three values for each $\alpha\beta$ pair. We have chosen the MSF to be the maximum of those values for each complex point.

IV. THREE-OSCILLATOR UNIVERSAL PROBE

We can calculate the MSF numerically for a great many systems, so long as we have a good model for the dynamics. However, it is sometimes easier or faster to vary experimental parameters than numerical ones, and in some cases the numerical model may not be accurate. In the cases where we can construct a network of the nodes we are interested in, *and* we can control the coupling weights to each node, we now show that there is a simple configuration of three nodes that will allow us to completely probe the MSF over the entire complex plane. This special configuration works because the three-oscillator array is the simplest array configuration which allows complex eigenvalues in the block structure of the system's variational equations. In the three-oscillator case the coupling is simultaneously nearest neighbor, all to all, and shift invariant (periodic boundary conditions).

Consider the following setup of three, coupled oscillators (we consider only additive coupling for now for simplicity):

$$\frac{d\mathbf{x}^i}{dt}=F(\mathbf{x}^i)+\frac{\varepsilon}{3}[\mathbf{H}(\mathbf{x}^{i+1})+\mathbf{H}(\mathbf{x}^{i-1})-2\mathbf{H}(\mathbf{x}^i)]$$
$$+\frac{\delta}{\sqrt{3}}[\mathbf{H}(\mathbf{x}^{i+1})-\mathbf{H}(\mathbf{x}^{i-1})],$$
$$(25)$$
$$i=1,2,3 \quad \text{cyclically,}$$

where we have added factors of 3 and $\sqrt{3}$ to simplify later equations. See Fig. 3 for a schematic of this configuration. The first term is a symmetric coupling and the second term an antisymmetric coupling. The variational equation is

$$\frac{d\boldsymbol{\xi}}{dt}=\begin{pmatrix} \mathbf{J} & 0 & 0 \\ 0 & \mathbf{J} & 0 \\ 0 & 0 & \mathbf{J} \end{pmatrix}\boldsymbol{\xi}+\begin{pmatrix} -2\dfrac{\varepsilon}{3} & \dfrac{\varepsilon}{3}+\dfrac{\delta}{\sqrt{3}} & \dfrac{\varepsilon}{3}-\dfrac{\delta}{\sqrt{3}} \\ \dfrac{\varepsilon}{3}-\dfrac{\delta}{\sqrt{3}} & -2\dfrac{\varepsilon}{3} & \dfrac{\varepsilon}{3}+\dfrac{\delta}{\sqrt{3}} \\ \dfrac{\varepsilon}{3}+\dfrac{\delta}{\sqrt{3}} & \dfrac{\varepsilon}{3}-\dfrac{\delta}{\sqrt{3}} & -2\dfrac{\varepsilon}{3} \end{pmatrix}$$
$$\otimes D\mathbf{H}\cdot\boldsymbol{\xi}. \qquad (26)$$

Diagonalizing the second term connection matrix ($\mathbf{G}$) gives

FIG. 2. Asymptotic form of the master stability function for small values of real coupling (a) when imaginary coupling (b) is large. The inset shows, schematically, how the surfaces associated with each Lyapunov exponent cross to give the form of the MSF shown.

$$\frac{d\boldsymbol{\psi}}{dt} = \begin{pmatrix} \mathbf{J} & 0 & 0 \\ 0 & \mathbf{J} & 0 \\ 0 & 0 & \mathbf{J} \end{pmatrix} \boldsymbol{\psi}$$

$$+ \begin{pmatrix} 0 & 0 & 0 \\ 0 & (\varepsilon+i\delta)D\mathbf{H} & 0 \\ 0 & 0 & (\varepsilon-i\delta)D\mathbf{H} \end{pmatrix} \boldsymbol{\psi}, \quad (27)$$

where ψ is ξ transformed to the eigencoordinates.

For the MSF we are only interested in the lower-right 2×2 block. Because of the symmetry of the MSF about the real axis, we only need one subblock, say for the $\varepsilon+i\delta$ block, to obtain the stability of the system. But we see that by varying ε and δ we can cover the entire complex plane. Hence we can probe the entire MSF using only a three-
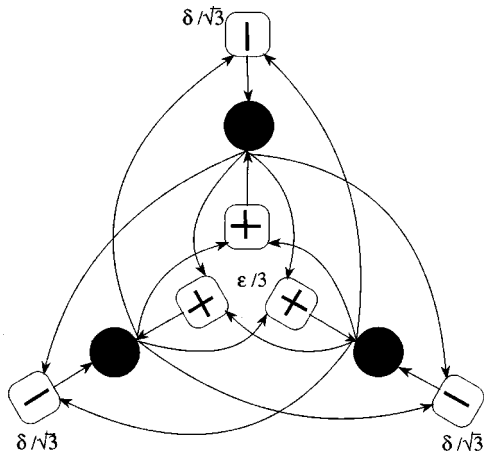
FIG. 3. Schematic of three oscillator system where each oscillator is connected to the two neighbors through the **H** function (lines with arrows) with combinations that are symmetric (+, with weight $\varepsilon/3$) and antisymmetric (−, with weight $\delta/\sqrt{3}$).
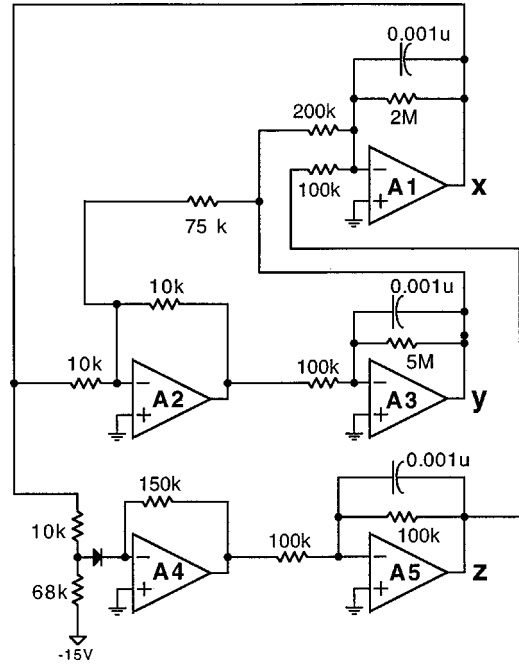
FIG. 4. Circuit schematic.

oscillator system. For that reason we call our coupling scheme involving the three oscillators a *universal probe of the master stability function*. This means that, given the node (the vector field **F**) and the coupling function (**H**) to apply to each node, the three-oscillator system above can probe the stability of *any* other configuration (**G**) of those oscillators. In Sec. V we apply the universal, three-oscillator probe to a circuit version of the Rössler system comparing the experimental probe of the MSF with the numerical results.

V. APPLICATION TO CIRCUIT-RÖSSLER SYSTEM

To rigorously demonstrate the practical usefulness of the three-oscillator universal probe of the MSF, we apply the above concepts to a physical system, a system complete with inherent parameter mismatch and noise. We have developed a fairly minimal electronic circuit which will be our testbed.

As our chaotic oscillators, we chose to use circuits modeled after the Rössler equations [36], where the quadratic nonlinearity is replaced by a piecewise linear function; we have also added an additional damping term to the ''x'' equation for electronic stability [5]. Figure 4 shows a schematic of this circuit. The oscillator circuits are described by [5]

$$\frac{dx}{dt} = -k(ax+by+cz),$$

$$\frac{dy}{dt} = -k(x+fy), \quad (28)$$

$$\frac{dz}{dt} = -k(-g(x)+z),$$
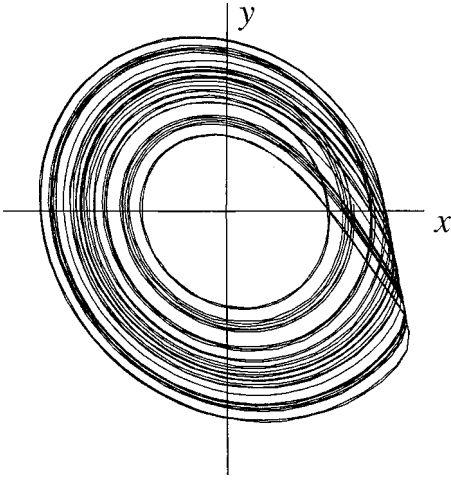
with

FIG. 5. x-y voltage plot of circuit attractor from time series.

$$g(x) = \begin{cases} 0, & x \leq 3 \\ h, & x > 3 \end{cases}.$$

For easy availability of componentry, the circuit was designed with the following parameters: $a = 0.05$, $b = 0.5$, $c = 1.0$, $f = 0.133$, and $h = 15$. The constant k is simply a time-scaling factor, which for our circuit is $10^4 \, s^{-1}$ Figure 5 shows an $x - y$ plot of the circuit oscillator generated from voltages of a running circuit. Numeric simulation of the equations above give an attractor that is very similar to Fig. 5.

On the complex plane for the MSF, the requirement for synchronization, the greatest Lyapunov exponent less than zero, defines a line or border. What we need now is a method to examine the stability and performance of synchronized systems on both sides of the ''threshold of synchronization.'' The chaotic nature of these systems makes demonstration of a synchronization threshold in a noisy physical system a particularly important step in the development of a robust theory, and yields an interesting deviation from that theory, which will be discussed later.

We construct a ring of three oscillators. In the electronic implementation of the universal system of Sec. IV, voltage coupling is accomplished by a series of operational amplifiers. First, the signal from each oscillator's x output is routed to an operational amplifier buffer; this assures that our coupling tap does not affect the operation of the running oscillators. Then each signal is routed to three of six operational amplifier adding arrays. The first three of the six generate the $(x^{j+1} + x^{j-1} - 2x^j)$ component, while the latter three subtract $(x^{j+1} - x^{j-1})$. A similar scheme is used for y coupling, with y^j replacing x^j. Finally, each signal is then multiplied by δ or ε respectively, by using an analog multiplier IC. The time delay caused by this process is negligibly short in relation to the time scale of our oscillators.

Thus we have our fully coupled circuit equations

$$\frac{d\mathbf{x}^j}{dt} = F(\mathbf{x}^j) + \mathbf{A}(\mathbf{x}^{j+1} + \mathbf{x}^{j-1} - 2\mathbf{x}^j) + \mathbf{B}(\mathbf{x}^{j+1} - \mathbf{x}^{j-1}),$$

$$(29)$$

along with their respective variational equations

$$\frac{d\xi_j}{dt} = \mathbf{J}(\mathbf{x}^j) \cdot \xi^j + \mathbf{A}(\xi^{j+1} + \xi^{j-1} - 2\xi^j) + \mathbf{B}(\xi^{j+1} - \xi^{j-1}),$$

$$(30)$$

where $\mathbf{F}$ is the vector field given by Eq. (28), and $\mathbf{J}$ is the Jacobian of Eq. (28). The matrices $\mathbf{A}$ and $\mathbf{B}$ are the symmetric and antisymmetric parts of the coupling, respectively, and are analogous to the ε and δ contributions, respectively, to Eq. (28). For x coupling the matrices $\mathbf{A}$ and $\mathbf{B}$ become

$$\mathbf{A} = \begin{pmatrix} \varepsilon & 0 & 0 \\ 0 & 0 & 0 \\ 0 & 0 & 0 \end{pmatrix}, \quad \mathbf{B} = \begin{pmatrix} \delta & 0 & 0 \\ 0 & 0 & 0 \\ 0 & 0 & 0 \end{pmatrix}, \quad (31)$$

and, for y coupling,

$$\mathbf{A} = \begin{pmatrix} 0 & 0 & 0 \\ 0 & \varepsilon & 0 \\ 0 & 0 & 0 \end{pmatrix}, \quad \mathbf{B} = \begin{pmatrix} 0 & 0 & 0 \\ 0 & \delta & 0 \\ 0 & 0 & 0 \end{pmatrix}. \quad (32)$$

which, except for the factors of 3, is equivalent to the $\mathbf{G}$ matrix of Eq. (26) when

$$D\mathbf{H} = \begin{pmatrix} 1 & 0 & 0 \\ 0 & 0 & 0 \\ 0 & 0 & 0 \end{pmatrix} \quad (33)$$

for x coupling, and

$$D\mathbf{H} = \begin{pmatrix} 0 & 0 & 0 \\ 0 & 1 & 0 \\ 0 & 0 & 0 \end{pmatrix} \quad (34)$$

for y coupling.

Observing the stability of the circuits in the component in which we are coupling would not give a true picture of what is happening, so data must be taken from a component other than the one by which the circuits are coupled. This allows us to see any pronounced bursting or other desynchronization effects which would be surpressed from observation in the coupled component, since the coupling tends to slave its components to each other, regardless of what the uncoupled components are doing. Thus, if the uncoupled component appears to be synchronized, we can be certain that the rest of the circuit is stably synchronized as well. We will observe the behavior of just the y component when coupling x, and observe just x when coupling y.

Observations, both in numeric simulation and in physical experiment, are made in orthogonal bases perpendicular to the plane of synchronization. We have shown that the transverse directions can be given by complex numbers as in Eq. (27); however, for experiment we need real numbers, so we choose two directions in real phase space that are transverse to the synchronization manifold. These are easy to find. All components are equal on the synchronization manifold which can be treated as a ''vector'' along the ''diagonal'' in phase space, namely, [1, 1, 1]. Two vectors orthogonal to this diagonal, and, therefore, spanning the transverse directions, are [2, −1, −1] and [0, −1, 1]. Thus in numeric simulation for x coupling, we recorded the separation S
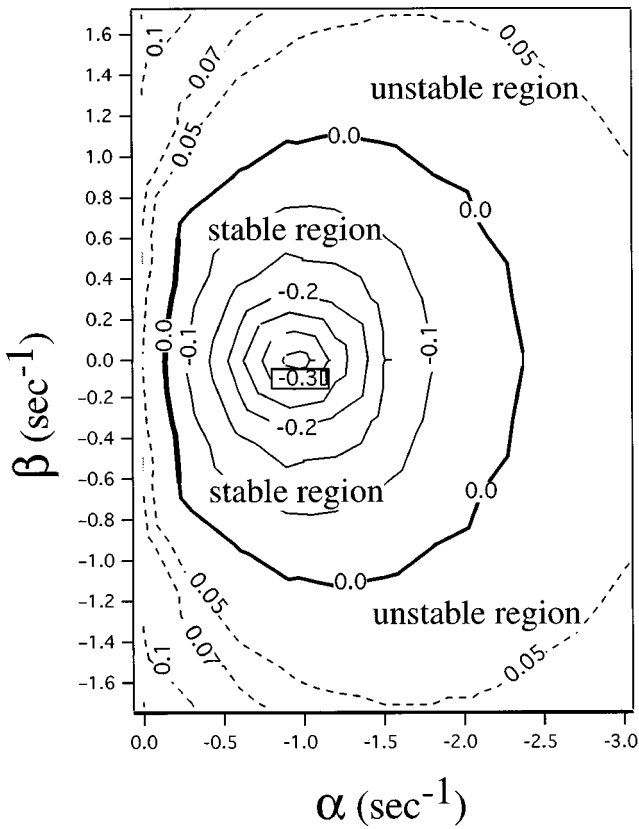
FIG. 6. The master stability function for x coupling, as per Eq. (33), in the Rössler circuit. The dashed lines show contours in the unstable region. The solid lines are contours in the stable region.

$$S_{\text{Theoretical}} = \sqrt{(2y^1 - y^2 - y^3)^2 + (y^3 - y^2)^2}. \qquad (35)$$

In the experiment, the separation between circuits was found by capturing only two streams of data, recording $(x_1 - x_2)$ as channel 1 C_1 and $(x_1 - x_3)$ as channel 2 (C_2). Substituting the expressions for the two channels into Eq. (35) gives,

$$S_{\text{Experimental}} = \sqrt{(C_1 + C_2)^2 + (C_1 - C_2)^2} \qquad (36)$$

Similar results obtain for y coupling with x^j replacing y^j.

The experiment was controlled and automated by a Lab-Windows based computer program, and proceeded as follows: An eight-bit digital to analog converter, controlled by the computer, supplied dc voltages to the two sets of multiplier chips: one for ε, and one for δ. An optimal ε and δ, determined in advance, were switched on and held for 0.1 sec (approximantely 100 cycles) insuring initial synchronization of the three oscillators. At the completion of this cycle, the voltages were simultaneously changed to new ε's and δ's. A few cycles later, $(10^{-2}$ s), a 12-bit analog to digital converter began to record the separation of the oscillators, as described in the paragraph above, for approximately 400 cycles. The results were then averaged, yielding a single value for the separation of the oscillators at that particular combination of δ's and ε's.
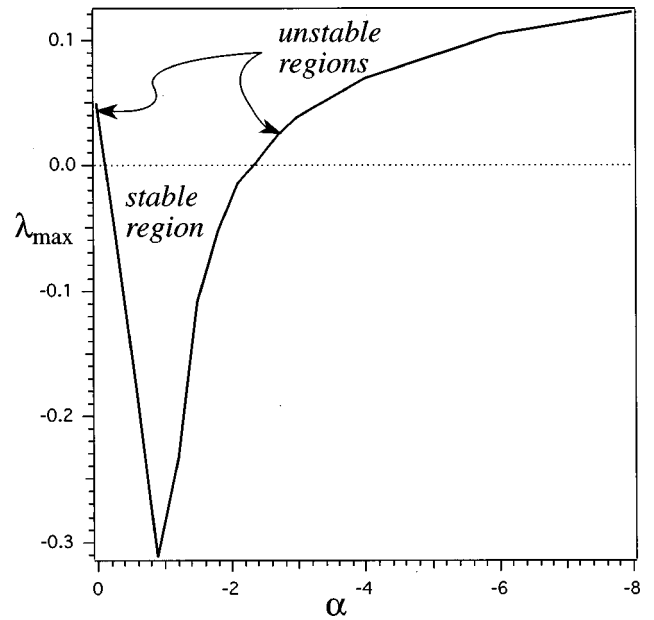
FIG. 7. One-dimensional plot of $\lambda_{\max}$ along the real axis (x coupling).

A. x coupling

Coupling the oscillators by their x components, we observed the output of the y components. Figure 6 shows a map of the maximum Lyapunov exponents as predicted by computer simulation. It suggests an elliptical shape for the stable region, always with increased stability along the real line where there is no antisymmetry. The shape of the MSF along the real line corresponds closely to earlier one-dimensional studies of Lyapunov exponents at varying coupling constants for symmetric diffusive coupling [5,34]. Figure 7 shows a one-dimensional plot of the theoretically predicted greatest Lyapunov exponent values.

Figure 8 presents the experimental version of the probe of the MSF using Eq. (36), with the same coupling scheme (x) as used in the circuits. There is no empirical link between the voltage scaling in theory and experiment, so that the scales of each may differ greatly. Within reasonable magnitudes, the shape and topology of the theory and experiment match well. Thus we have experimentally verified the shape of the stable region of the MSF.

B. y coupling

The above process was repeated, coupling the circuits via their y components, observing the outputs of the respective x components. Figures 9 and 10 show theory and experiment, respectively. As in the case of x coupling case, the topologies and shapes generally agree with each other, but here the curvature in the synchronization threshold reveals a weakness in using the Lyapunov exponents as a measure of synchronization stability.

The theoretical (Lyapunov exponent) threshold in the MSF runs almost vertically, parallel to the imaginary axis. The experimental threshold follows a parabolic shape. In the theoretical MSF such parabolic shapes occur in the contours at $\lambda_{\max}$ values that are negative. This would imply that in the experiment the y-coupling arrangement needs greater stability to cause robust synchronization. We take up this subject in the conclusions.
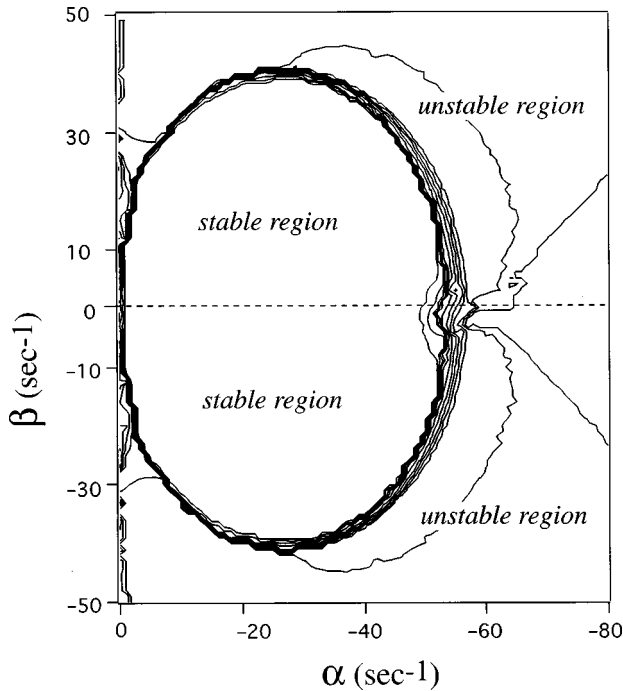
FIG. 8. Contour plot of experimental probe of the MSF (x coupling) using the synchronization distance measurement of Eq. (36). In the stable region the distances were below the threshold for synchronization. In the unstable region the distances were beyond the threshold for synchronization.

VI. CONCLUSIONS

The stability of many types of coupled systems can now be investigated at the same time. The only requirement is that the variational equation (not necessarily the original evolution equations) be of the form of a Jacobian of a node plus a weighted linear combination of Jacobians of the cou-
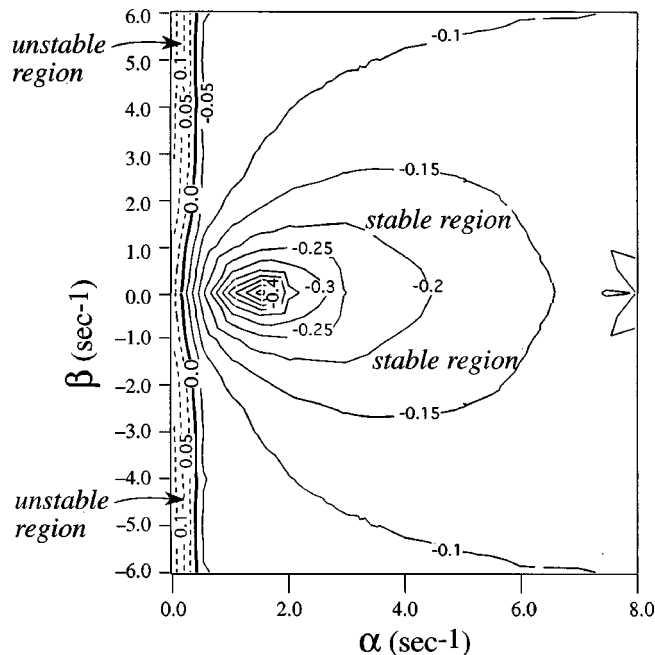
FIG. 9. The master stability function for y coupling, as per Eq. (34), in the Rössler circuit. The dashed lines show contours in the unstable region. The solid lines are contours in the stable region.
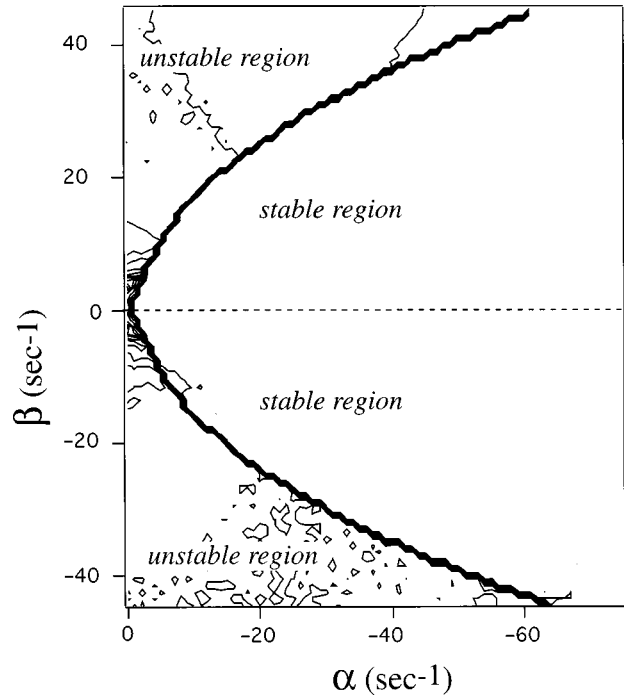
FIG. 10. Experimental probe of the MSF (y coupling) using the synchronization distance measurement of Eq. (36). In the stable region the distances were below the threshold for synchronization. In the unstable region the distances were beyond the threshold for synchronization.

pling functions to other nodes.

We have shown that the form of the variational equation also allows one to probe the master stability function with a simple three-oscillator array whose coupling is linear, and can be varied as to its symmetric and antisymmetric weights. This allows for experimental probes of the MSF, giving direct contact with what would otherwise be an abstract mathematical entity.

In the experimental study when we used y coupling we saw a discrepancy between theory and experiment. In explaining that difference here, we open up possibilities for other master stability functions, each depending on the synchronization criterion one chooses. Several other criteria for synchronization thresholds have been suggested. These are (1) the maximum Lyapunov exponent or Floquet multiplier for the least stable invariant set [7,28], e.g., an unstable periodic orbit in a chaotic attractor; (2) the average of the nonconstant part of the Jacobian and coupling compared to the linear parts [37]; (3) the maximum (supremum) of the real part of the eigenvalues of the (instantaneous) Jacobian (including the coupling terms) at all points or some representative set of points on the attractor [27,38] (e.g., when negative this function guarantees ultimate transverse-direction contraction everywhere on the attractor); and (4) the maximum eigenvalue of the (instantaneous) symmetrized Jacobian (including the coupling terms) at all points or some representative set of points on the attractor [10] (e.g., this guarantees monotone damping of transverse perturbations [39]).

All criteria (1)–(4) require calculation of quantities from the same variational equation as that used here for the maximum Lyapunov exponent criterion. Hence the same tech-

niques that led to the block structure of the Jacobian and coupling components that we developed here will work with (1)–(4). Thus, for each criterion there is a master stability function, and coupling changes will manifest themselves as motion of the eigenvalues on the complex plane just as above. Furthermore, for each criterion the analysis using the three-oscillator universal probe also holds. In this way the three-oscillator probe can be a good test for which criteria is best applicable to a particular system, by comparing the experiment with the master stability function for each criterion.

APPENDIX: MAP VERSION OF MASTER STABILITY FUNCTION

In this appendix we show that many forms of coupled map lattices studied in the literature also can generate a master stability function for the stability of the synchronized state. Several types of coupling are used to study coupled-map lattices. These are (1) coupling through added functions,

$$x_{n+1}^i = F(x_n^i) + \sum g_{ij} H(x_n^j); \tag{A1}$$

(2) coupling through added arguments,

$$x_{n+1}^i = F\left(x_n^i + \sum g_{ij} H(x_n^j)\right), \tag{A2}$$

and (3) general, nonlinear functional coupling,

$$x_{n+1}^i = F^i(x_n^i, \{H(x_n^j)\}), \tag{A3}$$

where the term in brackets stands for the output function H acting individually on each node in the array. In general, each node's map will be different in how it couples to other nodes, but the dynamics will be the same in the synchronous state. The form of the variational equations will be similar for all three coupled-map models. Letting $x^j = s$, the syn-

chronized value of the dynamical variables, these variational equations are, respectively, (1′) coupling through added functions,

$$\xi_{n+1}^i = \left[J(s_n) + \sum g_{ij} DH(s_n) \right] \xi_n^i, \tag{A4}$$

where J is the Jacobian of the first term, $F(x_n^i)$; (2′) coupling through added arguments,

$$\xi_{n+1}^i = \left[J(s_n) + \sum g_{ij} J(s_n) \cdot DH(s_n) \right] \xi_n^i, \tag{A5}$$

where we have made use of the usual chain rule for differentiation and the facts that $H(x_n^j) = H(s_n)$ for all j in the synchronous state and $\Sigma_{jg_{ij}} = 0$; and (3′) general, nonlinear functional coupling,

$$\xi_{n+1}^i = \left[J(s_n) + \sum g_{ij} DH(s_n) \right] \xi_n^i, \tag{A6}$$

where we assume that the individual functions F^i at each node have the same Jacobian with respect to the first argument (evaluated on the synchronization manifold), and that the derivatives (Jacobians) of F with respect to the other arguments (evaluated on the synchronization manifold) are all just multiples of the $m \times m$ unit matrix, i.e., they are the weights g_{ij}.

Thus all three forms, with suitable assumptions, are the same when the variational equations are evaluated on the synchronization manifold. That form is suitable for rewriting using direct products as in the ordinary differential equation (ODE) cases with a constant coupling matrix $G = \{g_{ij}\}$, and we can again carry through the diagonalization of G and extract the master variational equation leading to the master stability function for the coupled-map lattices. As in the ODE case, our choice of synchronization criterion will dictate which MSF we are calculating.

[1] H. Fujisaka and T. Yamada, Prog. Theor. Phys. **69**, 32 (1983).

[2] V. S. Afraimovich, N. N. Verichev, and M. I. Rabinovich, Izv. Vyssh. Uchebn. Zaved. Radio Fiz. **29**, 795–803 (1986).

[3] A. R. Volkovskii and N. F. Rul'kov, Sov. Tech. Phys. Lett. **15**, 249 (1989).

[4] J. M. Kowalski, G. L. Albert, and G. W. Gross, Phys. Rev. A **42**, 6260 (1990).

[5] J. F. Heagy, T. L. Carroll, and L. M. Pecora, Phys. Rev. E **50**, 1874 (1994).

[6] H. G. Winful and L. Rahman, Phys. Rev. Lett. **65**, 1575 (1990).

[7] P. Ashwin, J. Buescu, and I. Stewart, Phys. Lett. A **193**, 126 (1994).

[8] J. F. Heagy, T. L. Carroll, and L. M. Pecora, Phys. Rev. Lett. **73**, 3528 (1994).

[9] J. F. Heagy, T. L. Carroll, and L. M. Pecora, Phys. Rev. E **52**, R1253 (1995).

[10] D. J. Gauthier and J. C. Bienfang, Phys. Rev. Lett. **77**, 1751 (1996).

[11] A. S. Pikovskii, Radiophys. Quantum Electron. **27**, 390 (1984).

[12] N. Kopell and G. B. Ermentrout, Math. Biosci. **90**, 87 (1988).

[13] Y. Kuramoto, in *International Symposium on Mathematical Problems in Theoretical Physics*, edited by H. Araki, Lecture Notes in Physics Vol. 39 (Springer, Berlin, 1975), pp. 420–422.

[14] S. Watanabe and S. H. Strogatz, Phys. Rev. Lett. **70**, 2391 (1993).

[15] Steven Strogatz, *Nonlinear Dynamics and Chaos* (Addison-Wesley Publishing Co., Reading Massachusettes, 1994).

[16] S. H. Strogatz, in *Frontiers in Mathematical Biology*, edited by S. Levin (Springer, New York, 1994), Vol. 100, pp. 122–138.

[17] Chai Wah Wu and Leon O. Chua, Int. J. Bifurcation Chaos Appl. Sci. Eng. **4**, 979 (1994).

[18] C. W. Wu and L. O. Chua, IEEE Trans. Circuits Syst. **42**, 430 (1995).

[19] C. W. Wu and L. O. Chua, IEEE Trans. Circuits Syst., I: Fundam. Theory Appl. **43**, 161 (1996).

[20] D. Armbruster and G. Dangelmayr, Math. Proc. Cambridge Philos. Soc. **101**, 167 (1987).

[21] M. Golubitsky and I. Stewart, in *Multiparameter Bifurcation Theory, Contemporary Mathematics*, edited by M. Golubitsky

and J. Guckenheimer (American Mathematical Society, Providence, 1986), Vol. 56, pp. 131–173.

[22] V. Pérez-Villar *et al.*, Int. J. Bifurcation Chaos Appl. Sci. Eng. **3**, 1067 (1993).

[23] P. M. Gade, Phys. Rev. E **54**, 64 (1996).

[24] P. M. Gade, H. Cerdeira, and R. Ramaswamy, Phys. Rev. E **52**, 2478 (1995).

[25] Gang Hu, Junzhong Yang, and Winji Liu, Phys. Rev. E **58**, 4440 (1998).

[26] L. M. Pecora and T. L. Carroll, Phys. Rev. Lett. **80**, 2109 (1998).

[27] L. Pecora, T. Carroll, and J. Heagy (unpublished).

[28] N. F. Rulkov and M. M. Sushchik, Int. J. Bifurcation Chaos Appl. Sci. Eng. **7**, 625 (1997).

[29] G. H. Golub and C. F. Van Loan, *Matrix Computations* (The Johns Hopkins University Press, Baltimore, MD, 1996).

[30] L. M. Pecora *et al.*, Chaos **7**, 520 (1997).

[31] L. M. Pecora and T. L. Carroll, Phys. Rev. Lett. **64**, 821 (1990).

[32] L. M. Pecora and T. L. Carroll, Phys. Rev. A **44**, 2374 (1991).

[33] T. L. Carroll and L. M. Pecora, IEEE Trans. Circuits Syst. **38**, 453 (1991).

[34] J. F. Heagy, L. M. Pecora, and T. L. Carroll, Phys. Rev. Lett. **74**, 4185 (1995).

[35] J. A. Sanders and F. Verhulst, *Averaging Methods in Nonlinear Dynamical Systems* (Springer-Verlag, New York, 1985).

[36] O. E. Rössler, Phys. Lett. A **57**, 397 (1976).

[37] R. Brown and N. F. Rulkov, Phys. Rev. Lett. **78**, 4189 (1997).

[38] Similar criteria are used in control theory and are known as frozen Jacobian criteria. See W. L. Brogan, *Modern Control Theory* (Prentice-Hall, Englewood Cliffs, NJ, 1991).

[39] Tomasz Kapitaniak, Int. J. Bifurcation Chaos Appl. Sci. Eng. **6**, 211 (1996).